International Scholarly Research Network
ISRN Physical Chemistry
Volume 2012, Article ID 959074, 9 pages
doi:10.5402/2012/959074

Research Article

Design of Velocity Map Imaging Spectrometer Equipped with a Mass Gate Discriminating Particular Photofragments

Koichiro Mitsuke,[1,2] Hideki Katayanagi,[1,2] Bhim P. Kafle,[1] and Md. Serajul I. Prodhan[1]

[1] *Department of Photo-molecular Science, Institute for Molecular Science, Myodaiji, Okazaki 444-8585, Japan*
[2] *Department of Structural Molecular Science, Graduate University for Advanced Studies, Myodaiji, Okazaki 444-8585, Japan*

Correspondence should be addressed to Koichiro Mitsuke, nql47138@nifty.com

Received 29 January 2012; Accepted 15 March 2012

Academic Editors: C. L. Huang, H. Ihee, H. Saint-Martin, D. Strout, L. Vattuone, and S. Yang

A photoionization spectrometer for velocity map imaging has been developed for measuring the scattering distribution of fragment ions from polyatomic molecules. The spectrometer contains a mass gate and an ion reflector which are able to discriminate ions with a particular mass-to-charge ratio *m/z*. The basic functions and feasibility of these devices were tested experimentally and theoretically. First, the photoions from Kr and C_{60} were extracted into a time-of-flight (TOF) mass spectrometer by a transient or continuous electrostatic field. When the pulse application on the mass gate was tuned to the arrival timing of ions with a specific *m/z*, the peak of the selected ions alone was present on a TOF spectrum. Second, compatibility between velocity map imaging and ion discrimination was investigated by the computer simulations of the ion trajectories of photofragments from C_{60}. A pulsed voltage was applied to the mass gate synchronously with the arrival timing of C_{58}^+ ions. The initial three-dimensional velocity distribution of C_{58}^+ was projected onto the image plane with an energy resolution better than 10 meV. The C_{58}^+ image was free from the contamination of other ions such as C_{60}^+ and C_{56}^+.

1. Introduction

One can hardly discuss recent progress in photochemistry of gaseous molecules without stressing the development of the velocity map imaging (VMI) technique, as well as availability of powerful photon sources. In VMI the three-dimensional (3D) scattering distribution of photoelectrons or photoions is projected onto the surface of a position sensitive detector (PSD). The obtained image allows us to gain valuable insight into the dynamics of photoionization and photodissociation of fundamental small molecules [1–16]. General applications of VMI for polyatomic molecules should however await a practical solution [17, 18] to the following two problems. First, the image reflecting a characteristic scattering distribution of the fragment ions is almost smeared out due to the convolution of the thermal velocity of the parent ions. This effect becomes significant when the average barycentric velocity of the fragments is as low as that of the parent molecules [19]. Another difficulty arises when image data are contaminated by multiple fragments with different mass to charge ratio *m/z*. Some authors applied a pulsed high voltage to the front plate of the microchannel plate multipliers (MCP) just on time for the arrival of the ionic fragments with a particular *m/z* [20]. This MCP switching is not so advantageous to large molecules, because the time of flights of various kinds of fragments come close to one another. Furthermore, application of the pulsed high electric field brings about distortion of the equipotential surfaces inside a drift tube which prevents a part of ion trajectories from reaching the detector.

Recently, we proposed an idea of a VMI spectrometer modified for the cationic fragments from C_{60} photoionized with synchrotron radiation [21], based on the standard Eppink and Parker type lens system [3]. Originality of our apparatus lies in incorporation of a cylindrical mass gate and ion reflector inside the drift tube which is capable of discriminating the ions with a particular *m/z* (the ions of interest) from other unnecessary species. The distortion of the equipotential surfaces inside a drift tube can be minimized, since the pulsed voltage applied to the mass

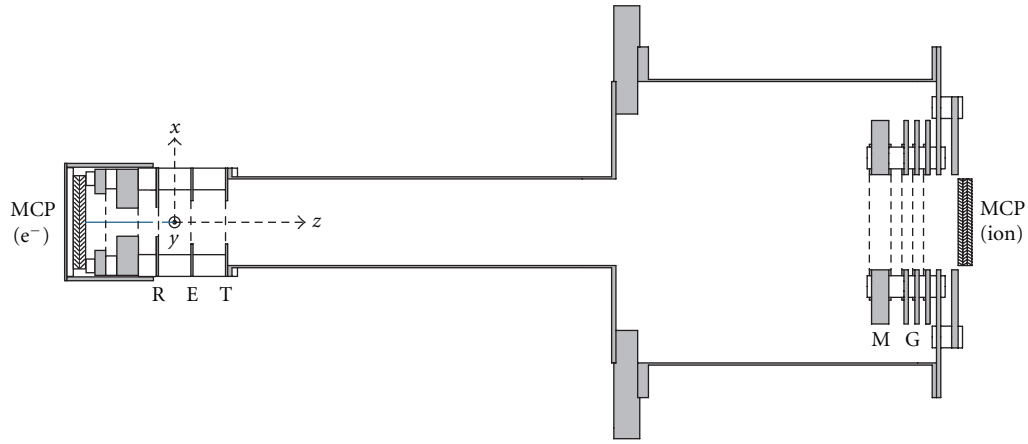

Figure 1: TOF mass spectrometer and electron analyzer. Synchrotron radiation was introduced along the y-axis. The dimensions of all the electrodes were determined from the computer simulation of ion/electron trajectories. R, repeller; E, ion extractor; T, tube entrance; M, mass gate; G, ion reflector.

gate is relatively low. This method may provide us with uncontaminated images of respective ionic fragments arising from large molecules, such as clusters, fullerenes, and biopolymers.

In the present paper, we will discuss the feasibility of the mass gate and ion reflector designed for VMI of photofragments from large molecules. Its capability for filtering the ions will be demonstrated in two ways. First, a basic function of the two devices will be tested experimentally by TOF mass spectrometry of Kr and C_{60}. Second, we will use computer simulation of the trajectories of fragment ions from C_{60} to show the performance of the two devices in discriminating the ions of interest, in the prospect of adaptation to the VMI studies. We will examine whether the pulsed operation of the mass gate has a negligible effect on the trajectories of the selected ions and whether the image on a PSD closely reflects their primary 3D velocity distribution.

2. Experimental

For the performance test of the mass gate and ion reflector, we used a conventional lens system of Wiley-McLaren type [22] including the electrodes of the repeller (R), ion extractor (E), and tube entrance (T) as shown in Figure 1. The ion extractor was separated by 15 mm from the other electrodes. All the electrodes are made of a racetrack-shaped titanium plate of thickness 1 mm. Central holes drilled in these electrodes were covered with fine meshes made of stainless steel. The tube-entrance electrode was fitted to a cylindrical drift tube of 340 mm long. The voltages applied to the respective electrodes and their dimensions are summarized in Table 1.

Monochromatized synchrotron radiation supplied from the bending magnet beamline BL2B in the UVSOR [23, 24] was focused using a post focusing mirror onto the center of the volume across which the repeller and ion-extractor electrodes face each other. The ambient pressure of the experimental chamber was ca. 7×10^{-8} Torr, but was increased to 2×10^{-6} Torr when the chamber was filled with gaseous Kr sample uniformly. The detailed explanation on our C_{60} beam source was given elsewhere [25]. The photoions produced by irradiation of synchrotron radiation were extracted by either (a) a pulsed electric field in the pulsed extraction (PEX) mode or (b) a continuous electrostatic field in the photoelectron photoion coincidence (PEPICO) mode. The ions were mass-separated by a double-focusing time-of-flight (TOF) mass spectrometer and detected with a z-stack MCP detectors (ϕ27 mm; Hamamatsu Photonics, F1552). A continuous voltage of -340 V was applied to the drift tube and its entrance, whereas the ion-extractor electrode was always kept grounded. The signal from MCP was processed by conventional pulse counting system and a time-to-digital converter with a minimum bin width of 1 ns (FastComtec, P7888).

In the PEX of Kr or C_{60}, a pulsed voltage rising from the ground level to $V_R = 75$ V was applied to the repeller electrode as a start trigger for the TOF measurement. The duration and frequency of the square wave pulse were 4.5 μs and 0.5–1.5 kHz, respectively. We chose the pulse amplitude to satisfy the Wiley-McLaren space-focusing condition: a good m/z resolution can be obtained at $V_R = 75$ V, together with the voltage settings of 0 and -340 V to the ion extractor and drift tube, respectively. Moreover, it is essential for us to keep the ionization region free from an electric field before the start trigger. Otherwise, TOF spectra suffer from serious peak broadening due to extraction of photoions prior to the rising edge of the pulsed voltage.

In the PEPICO of Kr, photoelectrons and photoions were accelerated in the opposite directions by a continuous electrostatic field between the repeller ($V_R = 75$ V) and ion extractor (0 V). Then the electrons passing through the central hole of the repeller were detected with another MCP (ϕ27 mm; Hamamatsu, F1552). The electron signal was amplified, discriminated, and fed into the start input of the time-to-digital converter.

The mass gate (M) and ion reflector (G) were installed in the end of the drift tube (see Figure 1); their symmetry axes agree with that of the drift tube. Their dimensions

Table 1: Voltages applied to the respective electrodes and their dimensions with internal diameter Φ.

Electrode	Voltages (V)		Dimensions (mm)	
	Base line value	Top line value[a]	Shape	Thickness or length
Repeller, R	0[b,c]	$V_R = 75$[b,c]	racetrack, [e]Φ = 20	1
	75[c,d]	—[c,d]		
Ion Extractor, E	0[b–d]	—	Racetrack, [e]Φ = 10	1
Tube Entrance, T	−340[b–d]	—	Racetrack, [e]Φ = 15	1
Drift Tube	−340[b–d]	—	cylinder, Φ = 40, Φ = 130	340 (length)
Mass Gate, M	−340[b,d]	$V_M = 100$[b,d]	cylinder, Φ = 44	10 (length)
	−340[c]	—[c]		
Retarding Grid, [f]G2	80[b,d]	—[b,d]	circle, Φ = 44	1
	0[c]	—[c]		

[a]Voltage at the top line of the pulse waveform. Not applicable in the case of a DC operation.
[b]For the PEX mode.
[c]For the control experiments.
[d]For the PEPICO mode.
[e]Axes of 50 × 66,
[f]Second disk electrode of the ion reflector G.

and positions were optimized by ion-trajectory simulation (see Section 4). The optimum distances from the ionization region were 335.5 and 370.5 mm to the center of the mass gate and entrance of the MCP, respectively. The inner diameter of the mass gate was 44 mm. The length of the mass gate, 10 mm, was so chosen as to accommodate all the fragment ions with a particular *m/z* inside this device. Fine meshes were mounted on the both ends of the mass gate, so that we could disregard the distortion of the equipotential surfaces due to a fringe effect. The ion reflector was composed of a triplet of disk electrodes that have central holes of 44 mm in diameter covered with fine meshes. The second disk electrode G2 named "retarding grid" was placed 5 mm apart from the first and third disk electrodes that were kept at −340 V (G1 and G3). These two electrodes made the equipotential surfaces flat and parallel inside the ion reflector. In Figure 1 all the electrodes with meshes have 85% transmission and the total transmission due to the 7 meshes in the full trajectory of photoions is 32%.

The retarding grid was biased to 80 V in both the PEX and PEPICO modes. Eventually, all ions were forced back there and unable to enter the MCP. We then applied a pulsed voltage changing from −340 V to V_M to the mass gate by using a home made pulse generator. Instantaneously the potential energies of the ions were elevated. The ions of interest were made to pass through the retarding grid and reach the MCP, if we had adjusted the application timing of V_M to their arrival time into the mass gate. Practically an optimum V_M value was searched by slowly increasing the amplitude until the ions of interest began to be observed and its count rate almost leveled off.

For the control experiment we applied DC voltages of −340 and 0 V to the mass gate and retarding grid, respectively. This combination resulted in no *m/z* discrimination and allowed all the ions to go beyond the ion reflector.

3. Results: Test of the Mass Gate

3.1. PEX of Kr. Figure 2 shows the TOF mass spectra of Kr^{z+} (z = 1–3) from Kr measured at $h\nu$ = 91 eV. Panel (a) was obtained by the control experiment in which a transient pulse changing from 0 to V_R = 75 V was applied to the repeller. The mass gate was set to a constant voltage of −340 V. Indeed all the species were observed with the MCP. A good signal to background ratio was attained because of the enhancement in photoionization cross section at the $3d^{-1}{}_{5/2}5p^1$ resonance of 91.2 eV.

The voltage settings for the PEX of Kr^{2+} were adopted in Panel (b): a pulsed voltage changing from −340 to V_M = +100 V was applied to the mass gate and a continuous voltage of 80 V to the retarding grid. The difference in application timing was 9 μs between the pulsed voltages of V_R and V_M. The pulse duration at the mass gate was 2 μs. Figure 2(b) exhibits a single peak of Kr^{2+} whose TOF position was nearly equal to the corresponding peak in Panel (a). Similarly, any ion could be discriminated according to its charged state using the mass gate and retarding grid.

3.2. PEPICO of Kr. Figure 3 shows the TOF mass spectra of Kr^{z+} from Kr measured at $h\nu$ = 91 eV. Panel (a) was obtained by the control experiment with continuous voltages of 75 and −340 V to the repeller and mass gate, respectively. Thus, no *m/z* discrimination was discernible. Here, the start triggers were taken from the photoelectron signals. The rate of background counts is higher in Figure 3(a) than in Figure 2(a), which is due to the false coincidence counts arising from the ion signal which has no time correlation with the electron triggers.

In Figure 3(b), the voltage settings for the PEPICO mode were employed. The timing of V_M was so chosen that the time lag with respect to the photoelectron trigger agrees

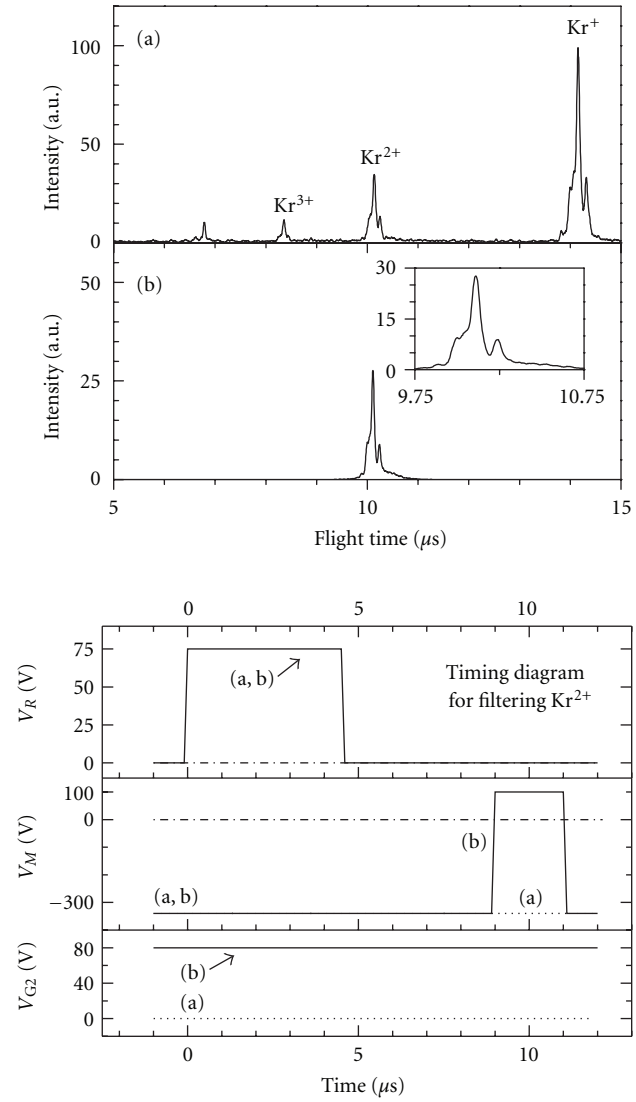

Figure 2: TOF spectra of Kr at $h\nu = 91$ eV (top) and the relevant timing diagram (bottom). (a) The control experiment by applying a pulse voltage to the repeller ($V_R = 75$ V); (b) the discrimination of Kr^{2+} by the PEX mode. The retarding grid was biased to 80 V, and a 100-V pulsed voltage was applied to the mass gate.

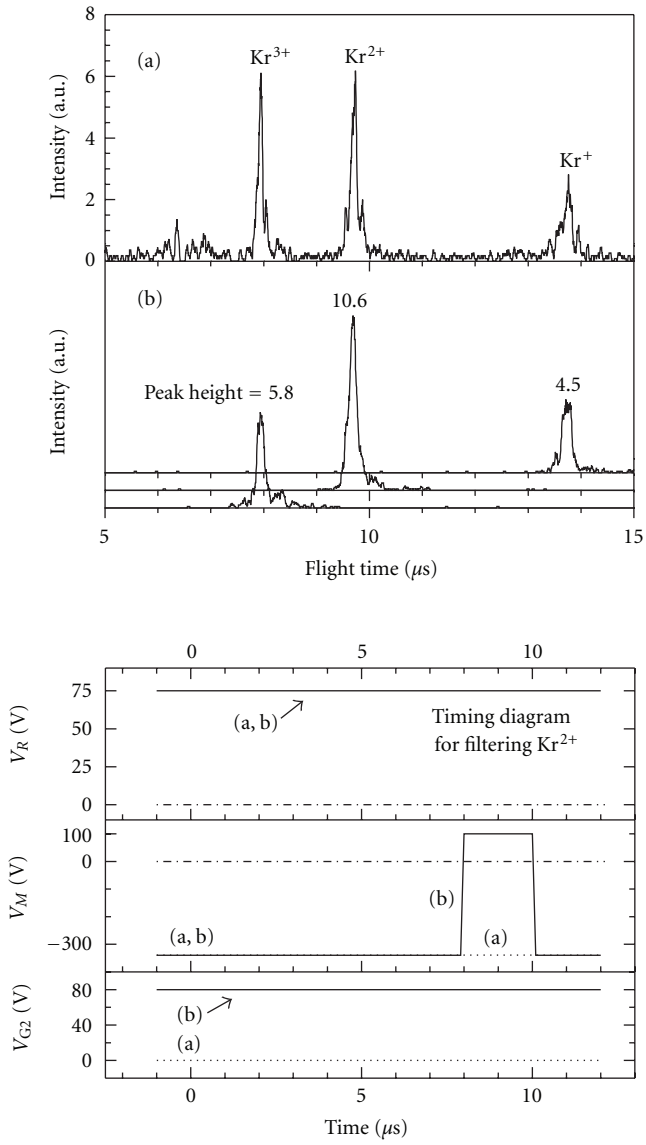

Figure 3: TOF spectra of Kr at $h\nu = 91$ eV (top) and the relevant timing diagram (bottom). (a) The control experiment with the photoelectron triggers. Acontinuous voltage of 75 V was applied to the repeller. (b) The discrimination of Kr^{z+} by the PEPICO mode. The retarding grid was biased to 80 V, and a 100-V pulsed voltage was applied to the mass gate.

with the flight time of the ions of interest. Indeed, the three spectra in Figure 3(b) obtained at the time lag of 6.2, 8.0, and 12.0 μs contain sharp peaks of Kr^{3+}, Kr^{2+}, and Kr^{+}, respectively. The mass resolving power in Figure 3(b) appears to be a little lower than that in Figure 2(b). The better mass resolution in the PEX mode arises from the so-called time-lag focusing [22] that is effective in the TOF mass spectrometer of Wiley-McLaren type.

The ratio between the intensity of Kr^{z+} ($z = 2$ or 3) to that of Kr^{+} was found to be higher in Figure 3(b) than the reported value [26] at $h\nu = 91$ eV. This is reasonably interpreted in terms of the difference in the number of detectable photoelectrons. In addition, the above discrepancy is probably ascribable to the dependence of the photoelectron detection efficiency on the electron kinetic energy.

3.3. PEX of C_{60}. Figure 4 shows the TOF mass spectra of C_{60} measured at $h\nu = 90$ eV. Panel (a) was obtained by the control experiment with applying a pulsed voltage of $V_R = 75$ V to the repeller. There are various photofragments, such as C_{58}^{2+}, C_{56}^{2+}, and C_{54}^{2+}, in addition to the strong peaks of C_{60}^{z+} ($z = 1$–3). In contrast, the voltage settings for the PEX of particular ions were adopted in Panels (b) and (c): pulsed (-340 V $\rightarrow$ $+100$ V) and static (80 V) voltages were fed to the mass gate and retarding grid, respectively. In Panel (b) the time interval from the leading edge of the V_R pulse to that of the V_M pulse was 24 μs and the duration of V_M was 3 μs. These time interval and duration were set in Panel (c) to 24.7 and 0.7 μs, respectively. The parent and fragment

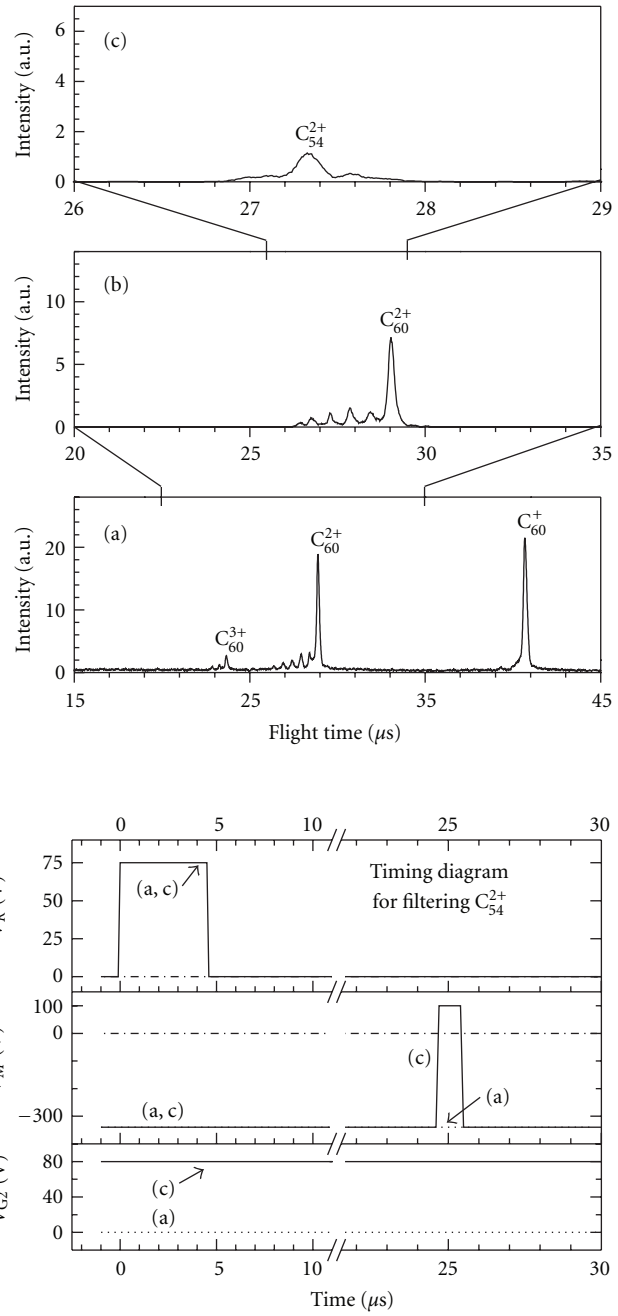

FIGURE 4: TOF spectra of C_{60} at $h\nu = 90$ eV (top) and the relevant timing diagram (bottom). (a) The control experiment by applying apulsed voltage to the repeller ($V_R = 75$ V); (b) and (c) the discrimination of all species in doubly-charged state and $C_{54}{}^{2+}$, respectively, by the PEX mode. The retarding grid was biased to 80 V, and a 100-V pulsed voltage was applied to the mass gate.

ions in doubly charged state alone remain in Panel (b). With the narrower duration, only the fragment peak of $C_{54}{}^{2+}$ could be selected in Panel (c). Obviously we have achieved the mass resolving power high enough to discriminate the ions of interest from the mixture of the multiple fragment ions.

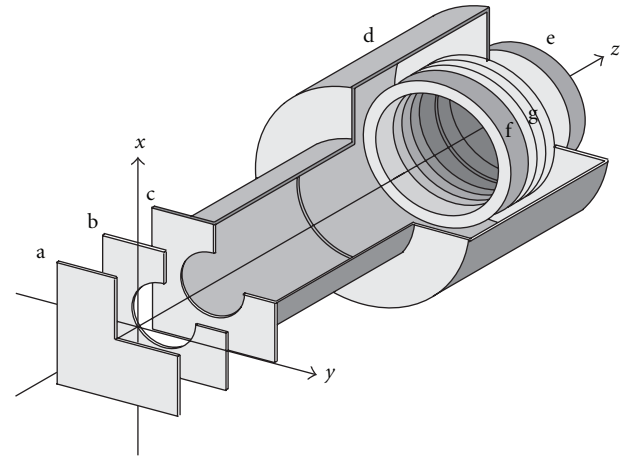

FIGURE 5: Schematic view of the VMI spectrometer used for the computer simulations of ion trajectories. Synchrotron radiation was introduced along the y-axis. a, repeller; b, ion extractor; c, tube entrance; d, drift tube; e, PSD; f, mass gate; g, ion reflector.

4. Trajectory Simulations of the VMI Spectrometer

4.1. Basic Idea of the Simulation. We have demonstrated in Section 3 that the mass gate and ion reflector fulfill the function of filtering the ions with a particular m/z. The crucial point of our ion-discrimination method is the waveform of the voltage applied to the mass gate, that is, a positive-going square wave pulse with a negative DC offset. The base line value of -340 V is required to avoid any voltage discontinuity between the drift tube and mass gate. The top line value, $V_M = 100$ V, is determined at the demand of the ion-discrimination condition that the ions of interest gain a potential energy large enough to pass through the retarding grid. The amplitude (440 V) of the waveform used for switching our mass gate is much lower than that for switching the front plate of an MCP detector [20, 27]. Conducting ion filtering using low-amplitude pulses is particularly beneficial to VMI experiments because a rapid voltage change may easily distort the equipotential surfaces inside a drift tube. Therefore, the VMI spectrometer equipped with the present type of mass gate is expected to be useful in analyzing the 3D velocity distributions of various photofragments simultaneously produced. In what follows a possible performance of the mass gate inside the VMI spectrometer is investigated by the computer simulation of the ion trajectories. Taking an example of $C_{58}{}^{+}$ from C_{60} we have studied how low we can reduce the amplitude of the pulsed voltage applied to the mass gate with preserving a strict m/z discrimination and a high position resolution of the PSD.

For the trajectory simulation we replaced the ion lens system of Wiley-McLaren type in Figure 1 with that of VMI as displayed in Figure 5. Also the MCP was replaced with a PSD (ϕ40 mm). The arrangements of the two lens system in Figures 1 and 5 are similar to each other: both contain the repeller, ion-extractor and tube-entrance electrodes. In the simulation every electrode was assumed to have the dimensions listed in Table 1. The ion-extractor, and tube-entrance

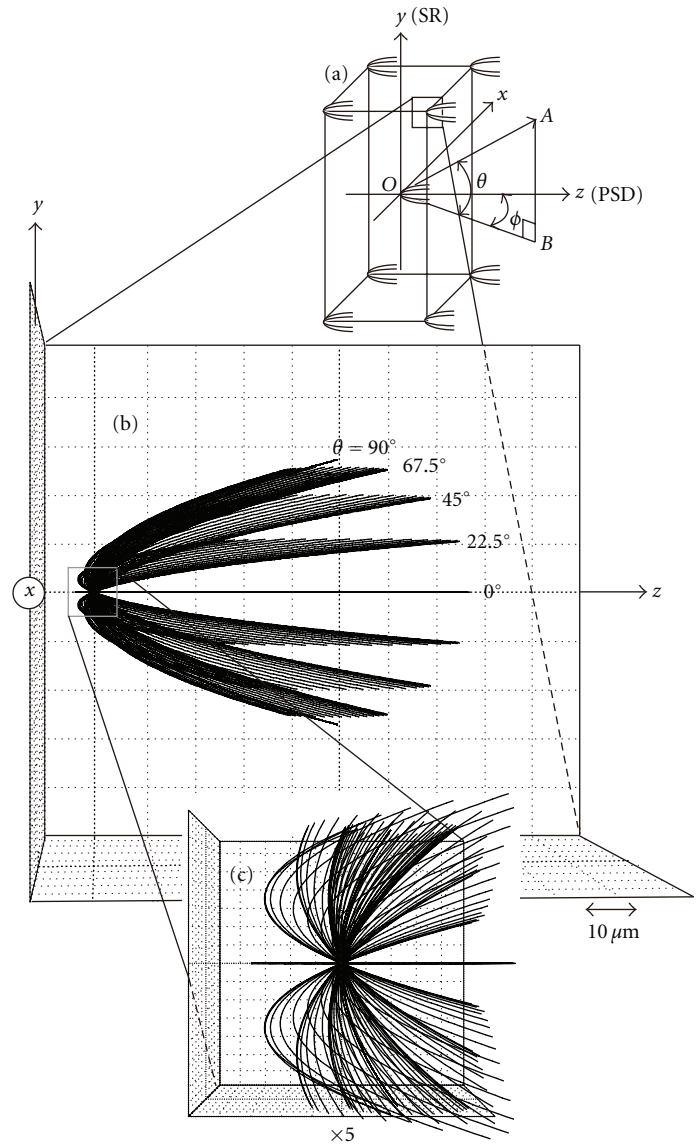

FIGURE 6: (a) Ionization volume and coordinate system defined for the simulations (not to scale). OA, ion emission direction; OB, projection of OA on the x- z plane; θ, elevation angle; ϕ, azimuth angle. (b) Ion trajectories starting from the point $(x, y, z) = (-0.5, 1.5, 0.5)$. (c) Expansion of (b) near the starting points of the ion flights.

electrodes have central holes of 20 mm in diameter with no mesh. Such open-hole structure of the two electrodes enables us to bend the equipotential surfaces simply by manipulating the ion-extractor voltage and to achieve the excellent focusing of the velocity map image on the PSD [3, 21, 28]. The separation between the ion extractor and the other electrodes was optimized from the simulation to be 15 mm.

4.2. Method of the Simulation. We performed ion trajectory simulations utilizing the SIMION 3D software (ver. 7.0) [29] to optimize the dimensions of the electrodes in Figure 5. The grid size of 0.5 or 1 mm was adopted in the simulations to keep a good scale factor. Here, dissociative ionization of C_{60} was considered to take place within a region of rectangular parallelepiped $\Delta x \Delta y \Delta z = 1 \times 3 \times 1\,\text{mm}^3$ as depicted in Figure 6(a). The y-direction was assigned to the propagation vector of synchrotron radiation, so that the y coordinate of the ionization region ranges from -1.5 to $+1.5$ mm.

In the trajectory simulations the eight corners and center of the ionization region were chosen for the starting points of the ion flights. From each point 171 trajectories were generated in the range of the elevation angle θ from –90° to +90° at intervals of 22.5° and in the range of the azimuth angle ϕ from 0° to +180° at intervals of 10°. The definition of the two angles is given in Figure 6(a).

Application of the pulsed voltages to the repeller and mass gate was realized by means of a "user program" of SIMION [29]. A pulsed voltage rising from the ground level to $V_R = 86$ V was applied to the repeller. The duration of the square wave pulse was 7 μs. The ion extractor was kept grounded, whereas the tube entrance was biased to -214 V.

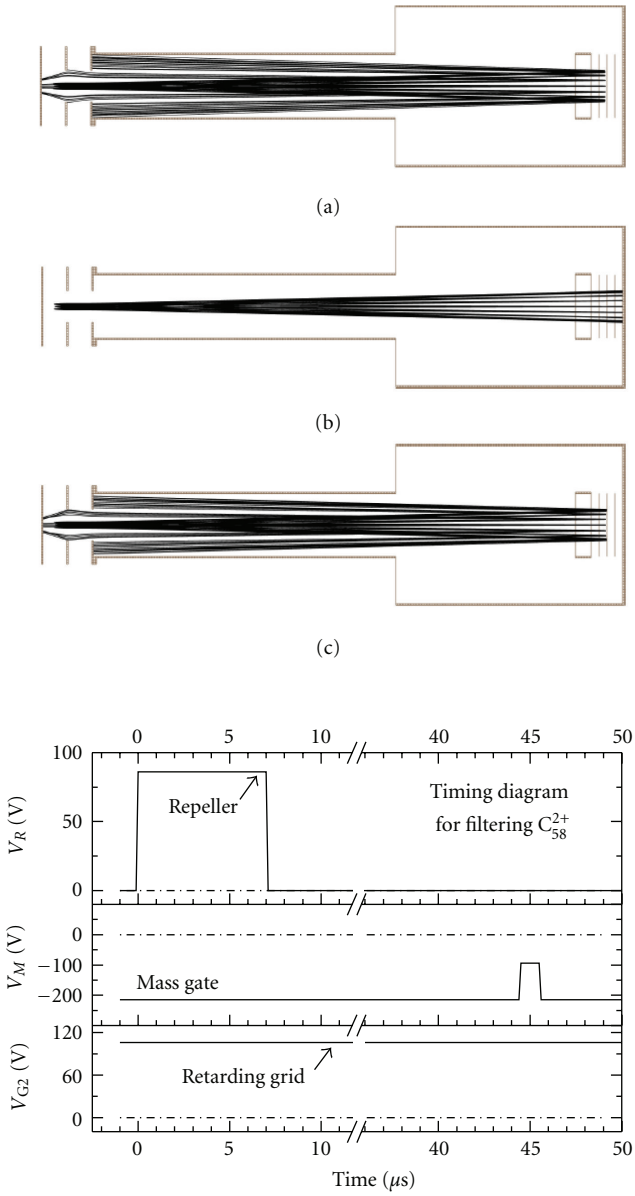

FIGURE 7: Simulated trajectories of (a) C_{60}^+, (b) C_{58}^+, and (c) C_{56}^+ produced from C_{60}. The initial kinetic energies of the ions were set to 0.1 eV. A pulsed voltage changing from −214 to −94 V was applied to the mass gate synchronously with the arrival timing of C_{58}^+ ions. Increase in their potential energies allows C_{58}^+ to pass through the retarding grid. The trajectories of C_{58}^+ can reach the PSD, whereas those of C_{60}^+ and C_{56}^+ turn around at the retarding grid and travel in the opposite direction. They terminate partly at the repeller electrode.

This combination of the voltages permits the scattered ions produced during the past 13 μs, with respect to the rising edge of the pulsed V_R voltage, to be guided into the drift tube. To filter C_{58}^+ ions we determined the timing of the pulsed voltage to the mass gate at 44.5 μs later than that to the repeller. At the mass gate the spread of the TOF of C_{58}^+ was estimated to be 0.65 μs which arises from the finite volume of the ionization region and distribution of the kinetic energy

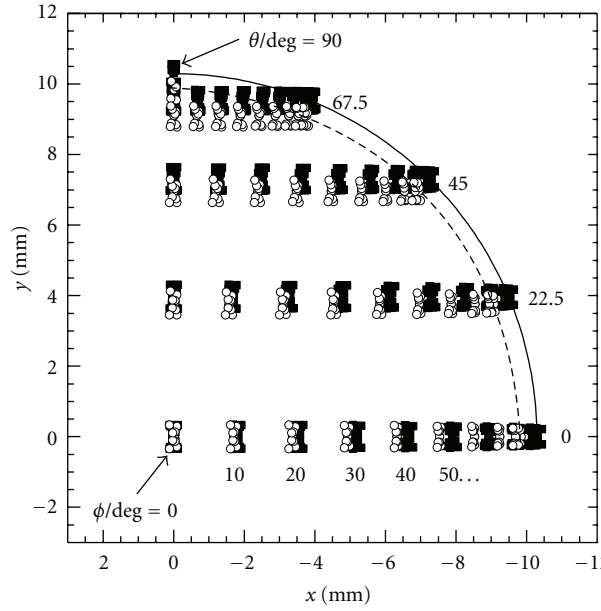

FIGURE 8: Simulated two-dimensional images of the three-dimensional velocity distribution of C_{58}^+ from C_{60} projected on the PSD. The initial kinetic energies of C_{58}^+ were set to 0.1 (◯) and 0.11 eV (■).

of the fragment ions. Thus, we applied a pulsed voltage 1 μs wide and 120 V high that changes from −214 to −94 V. A continuous voltage of 106 V was applied to the retarding grid of the ion reflector.

4.3. Simulation Results on C_{58}^+ from C_{60}. The simulated trajectories of C_{58}^+ at initial kinetic energies of 0.1 eV are illustrated in Figure 7(b), while those of C_{60}^+ and C_{56}^+ are in Figures 7(a) and 7(c), respectively. Most of the trajectories of C_{58}^+ are found to go beyond the retarding grid and reach the PSD, whereas the trajectories of C_{60}^+ and C_{56}^+ are reflected completely. This observation may provide evidence for exclusive imaging detection of C_{58}^+ without interference from the neighboring ions, C_{60}^+ and C_{56}^+, with the same kinetic energies.

Figure 8 shows the simulated velocity map images of C_{58}^+ ions on the PSD at the kinetic energies of 0.1 eV (open circles) and 0.11 eV (filled squares). It should be noted that these images result from momentum distributions of the ions in the laboratory system. We took into account the ion trajectories generated in the elevation and azimuth angle ranges of 0° to +90° and 0° to +180°, respectively, which cover only one quarter of the full three-dimensional trajectories over the 4π solid angle.

The trajectories with a given elevation angle form a horizontal stripe, and the envelope of all the stripes makes an arc, which clearly demonstrates that scattering distribution in spherical symmetry can be successfully projected on an image plane. It is likely that C_{58}^+ fragment ions with kinetic energy difference of 0.01 eV are almost separable. Comparison between the simulations with and without the

mass gate and ion reflector confirmed that the images are not distorted in the presence of these devices.

5. Conclusion

The results of the mass spectrometric experiments of Kr and C_{60} (Sections 2 and 3) and the ion trajectory simulations of C_{60} (Section 4) have clearly demonstrated the capability of the mass gate and ion reflector in discriminating specific ion species. We consider that the VMI for photofragmentation of fullerenes and large molecules is feasible by the use of the imaging spectrometer equipped with these two devices (see Figure 5). Practically, compensation lenses are needed between the ion-extractor and tube-entrance electrodes, because we must reduce the penetration of the external field arising from a beam source of fullerene and a thickness monitor. This point has been closely examined using the simulations on an improved spectrometer having four-element velocity focusing lens system. The details of the simulations will be published in a separate paper.

Acknowledgments

The authors are grateful to Drs. Chaoqun Huang and Hajime Yagi for their help in the beginning stage of the experiments. They also thank the members of the UVSOR for their help in the course of the experiments. This work has been supported by national funds appropriated for special research projects of the Institute for Molecular Science, by Grants-in-Aid for Scientific Research (Grant nos. 17750023, 18350016, 18045031, and 20550029) from the Ministry of Education, Culture, Sports, Science and Technology, Japan.

References

[1] D. W. Chandler and P. L. Houston, "Two-dimensional imaging of state-selected photodissociation products detected by multiphoton ionization," *Journal of Chemical Physics*, vol. 87, no. 2, pp. 1445–1447, 1987.

[2] P. L. Houston, "New laser-based and imaging methods for studying the dynamics of molecular collisions," *Journal of Physical Chemistry*, vol. 100, no. 31, pp. 12757–12770, 1996.

[3] A. T. J. B. Eppink and D. H. Parker, "Velocity map imaging of ions and electrons using electrostatic lenses: application in photoelectron and photofragment ion imaging of molecular oxygen," *Review of Scientific Instruments*, vol. 68, no. 9, pp. 3477–3484, 1997.

[4] D. S. Peterka, M. Ahmed, C. Y. Ng, and A. G. Suits, "Dissociative photoionization dynamics of SF6 by ion imaging with synchrotron undulator radiation," *Chemical Physics Letters*, vol. 312, no. 2–4, pp. 108–114, 1999.

[5] M. Takahashi, J. P. Cave, and J. H. D. Eland, "Velocity imaging photoionization coincidence apparatus for the study of angular correlations between electrons and fragment ions," *Review of Scientific Instruments*, vol. 71, no. 3, pp. 1337–1344, 2000.

[6] C. R. Gebhardt, T. P. Rakitzis, P. C. Samartzis, V. Ladopoulos, and T. N. Kitsopoulos, "Slice imaging: a new approach to ion imaging and velocity mapping," *Review of Scientific Instruments*, vol. 72, no. 10, pp. 3848–3853, 2001.

[7] H. L. Offerhaus, C. Nicole, F. Lépine, C. Bordas, F. Rosca-Pruna, and M. J. J. Vrakking, "A magnifying lens for velocity map imaging of electrons and ions," *Review of Scientific Instruments*, vol. 72, no. 8, pp. 3245–3248, 2001.

[8] L. Dinu, A. T. J. B. Eppink, F. Rosca-Pruna, H. L. Offerhaus, W. J. Van der Zande, and M. J. J. Vrakking, "Application of a time-resolved event counting technique in velocity map imaging," *Review of Scientific Instruments*, vol. 73, no. 12, pp. 4206–4213, 2002.

[9] J. J. Lin, J. Zhou, W. Shiu, and K. Liu, "Application of time-sliced ion velocity imaging to crossed molecular beam experiments," *Review of Scientific Instruments*, vol. 74, no. 4, pp. 2495–2500, 2003.

[10] B. Baguenard, J. B. Wills, F. Pagliarulo et al., "Velocity-map imaging electron spectrometer with time resolution," *Review of Scientific Instruments*, vol. 75, no. 2, pp. 324–328, 2004.

[11] G. A. Garcia, L. Nahon, C. J. Harding, E. A. Mikajlo, and I. Powis, "A refocusing modified velocity map imaging electron/ion spectrometer adapted to synchrotron radiation studies," *Review of Scientific Instruments*, vol. 76, no. 5, Article ID 053302, 11 pages, 2005.

[12] Y. Hikosaka and E. Shigemasa, "Velocity imaging spectrometer for negative fragment ions: application to dynamics of O_2 and N_2O ion-pair dissociation," *Journal of Electron Spectroscopy and Related Phenomena*, vol. 148, no. 1, pp. 5–10, 2005.

[13] B. D. Leskiw, M. H. Kim, G. E. Hall, and A. G. Suits, "Reflectron velocity map ion imaging," *Review of Scientific Instruments*, vol. 76, no. 12, pp. 104101–104106, 2005.

[14] A. Hishikawa, A. Matsuda, M. Fushitani, and E. J. Takahashi, "Visualizing recurrently migrating hydrogen in acetylene dication by intense ultrashort laser pulses," *Physical Review Letters*, vol. 99, no. 25, Article ID 258302, 4 pages, 2007.

[15] D. Rolles, Z. D. Pešić, M. Perri et al., "A velocity map imaging spectrometer for electron-ion and ion-ion coincidence experiments with synchrotron radiation," *Nuclear Instruments and Methods in Physics Research, Section B*, vol. 261, no. 1-2, pp. 170–174, 2007.

[16] H. Fukuzawa, K. Motomura, X. J. Liu et al., "Ion momentum spectroscopy of N_2 and O_2 molecules irradiated by EUV free-electron laser pulses," *Journal of Physics B*, vol. 42, no. 18, Article ID 181001, 2009.

[17] H. Fukuzawa, K. Motomura, X. J. Liu et al., "Ion momentum spectroscopy of N_2 and O_2 molecules irradiated by EUV free-electron laser pulses," *Journal of Physics B-Atomic Molecular and Optical Physics*, vol. 42, no. 18, Article ID 181001, 2009.

[18] H. Katayanagi and K. Mitsuke, "Mass-analyzed velocity map imaging of thermal photofragments from C_{70}," *Journal of Chemical Physics*, vol. 135, no. 14, Article ID 144307, 8 pages, 2011.

[19] M. S. I. Prodhan, H. Katayanagi, C. Huang, H. Yagi, B. P. Kafle, and K. Mitsuke, "Velocity map imaging apparatus applicable to a study of multiple photofragmentation of C_{60}," *Chemical Physics Letters*, vol. 469, no. 1–3, pp. 19–25, 2009.

[20] F. Aguirre and S. T. Pratt, "Ion-imaging of the photodissociation of CF_3I^+," *Journal of Chemical Physics*, vol. 118, no. 14, pp. 6318–6326, 2003.

[21] B. P. Kafle, H. Katayanagi, and K. Mitsuke, "Photofragment imaging apparatus for measuring momentum distributions in dissociative photoionization of fullerenes," in *Synchrotron Radiation Instrumentation*, J. Y. Choi and S. Rah, Eds., chapter 1, pp. 1809–1812, American Institute of Physics, Seoul, Korea, 2007.

[22] W. C. Wiley and I. H. McLaren, "Time-of-flight mass spectrometer with improved resolution," *Review of Scientific Instruments*, vol. 26, no. 12, pp. 1150–1157, 1955.

[23] M. Ono, H. Yoshida, H. Hattori, and K. Mitsuke, "Performance of the 18 m-spherical grating monochromator newly developed in the UVSOR facility," *Nuclear Instruments and Methods in Physics Research, Section A*, vol. 467-468, pp. 577–580, 2001.

[24] H. Yoshida and K. Mitsuke, "Design of an 18 m spherical-grating monochromator at UVSOR," *Journal of Synchrotron Radiation*, vol. 5, no. 3, pp. 774–776, 1998.

[25] T. Mori, J. Kou, M. Ono, Y. Haruyama, Y. Kubozono, and K. Mistuke, "Development of a photoionization spectrometer for accurate ion yield measurements from gaseous fullerenes," *Review of Scientific Instruments*, vol. 74, no. 8, pp. 3769–3773, 2003.

[26] N. Saito and I. H. Suzuki, "Multiple photoionization in Ne, Ar, Kr and Xe from 44 to 1300 eV," *International Journal of Mass Spectrometry and Ion Processes*, vol. 115, no. 2-3, pp. 157–172, 1992.

[27] F. Aguirre and S. T. Pratt, "Velocity map imaging of the photodissociation of CF_3I: vibrational energy dependence of the recoil anisotropy," *Journal of Chemical Physics*, vol. 118, no. 3, pp. 1175–1183, 2003.

[28] B. Tang and B. Zhang, "Photodissociation pathways and dissociation energy of C-Br bond of n-C_4H_9Br determined using velocity map imaging," *Chemical Physics Letters*, vol. 412, no. 1–3, pp. 145–151, 2005.

[29] D. A. Dahl, *SIMION 3D 7.0*, Scientific Instrument Services, Boise, Idahom USA, 2000.